Establishing Rod-Shape from Spherical, Peptidoglycan-Deficient Bacterial Spores

Huan Zhang[1], Garrett A. Mulholland[1], Sofiene Seef[2], Shiwei Zhu[3,4], Jun Liu[3,4], Tâm Mignot[2] and Beiyan Nan[1]*

[1]Department of Biology, Texas A&M University, College Station, TX 77843, USA
[2]Laboratoire de Chimie Bactérienne, CNRS - Université Aix Marseille UMR7283, Institut de Microbiologie de la Méditerranée, 13009 Marseille, France
[3]Department of Microbial Pathogenesis, Yale University School of Medicine, New Haven, CT 06536, USA
[4]Microbial Sciences Institute, Yale University, West Haven, CT 06516, USA

*Corresponding author: Beiyan Nan, 306C BSBE, 3258 TAMU, College Station, TX77843, Tel.: 979-845-3487, email: bnan@tamu.edu

Keywords: germination, Rod system, MreB, GTPase, gliding motility

ABSTRACT

Chemical-induced spores of the Gram-negative bacterium *Myxococcus xanthus* are peptidoglycan (PG)-deficient. It is unclear how these spherical spores germinate into rod-shaped, walled cells without preexisting PG templates. We found that germinating spores first synthesize PG randomly on spherical surfaces. MglB, a GTPase activating protein, surveys the status of PG growth and establishes one future cell pole. Following MglB, the Ras family GTPase MglA localizes to the second pole. MglA directs molecular motors to transport the bacterial actin homolog MreB and the Rod PG synthesis complexes away from poles. The Rod system establishes rod-shape by elongating PG at nonpolar regions. Thus, the interaction between GTPase, cytoskeletons and molecular motors provides a mechanism for the *de novo* establishment of rod-shape in bacteria.

Significance

Spheres and rods are among the most common shapes adopted by walled bacteria, in which the peptidoglycan (PG) cell wall largely determines cell shape. When induced by chemicals, rod-shaped vegetative cells of the Gram-negative bacterium *Myxococcus xanthus* thoroughly degrades their PG and shrinks into spherical spores. As these spores germinate, cells rebuild rod-shaped PG without preexisting templates, which provides a rare opportunity to visualize *de novo* PG synthesis and bacterial morphogenesis. In this study, we investigated how spherical spores elongation into rods during germination and elucidated a system for rod-shape morphogenesis that includes the Rod PG synthesis system, a GTPase-GAP pair, the MreB cytoskeleton and a molecular motor.

Morphogenesis is a fundamental problem in biological systems. Compared to symmetric spheres, rods are asymmetric and polarized. For most rod-shaped bacteria, the peptidoglycan (PG) cell wall defines cell geometry, which is synthesized by two major enzymatic systems. The Rod system consists of RodA, a SEDS-family PG polymerase, PBP2, a member of the class B penicillin-binding proteins (bPBPs), and MreB, a bacterial actin homolog (1-3). MreB orchestrates PG growth by the Rod complexes in response to local cell curvature (4-9). In contrast, class A PBPs (aPBPs) contribute to PG growth independent of MreB (10, 11).

Myxococcus xanthus, a rod-shaped Gram-negative bacterium, utilizes polarized geometry for directed locomotion. MglA, a Ras family small GTPase, controls the direction of gliding motility. The motors for gliding assemble into functional machineries on MreB filaments (12-16). Consequently, the gliding machineries carry MreB filaments as they move rapidly in the membrane (17). As cells move, GTP-bound MglA forms large clusters at leading cell poles, whereas GDP-bound MglA distributes homogeneously in the cytoplasm (16, 18, 19). The activity of MglA is regulated by its cognate GTPase-activating protein (GAP), MglB, which forms large clusters at lagging cell poles. MglB activates the GTPase activity of MglA, expelling MglA-GTP from lagging poles (18, 19). MglA regulates the assembly and moving direction of the gliding machinery through direct interaction with MreB (16, 20). Overall, the polarized localization and activities of MglA and MglB ensure that the majority of gliding machineries moves from poles to nonpolar regions, which generates propulsion (12, 16, 20).

Some rod-shaped bacteria change their geometry through sporulation. In Firmicutes such as Bacilli and Clostridia, the morphological differentiation from rod-shaped vegetative cells to oval spores begins with an asymmetric division, resulting in the formation of a smaller spore wholly contained within a larger mother cell. In contrast to endospore-forming bacteria, *M. xanthus* produces spores using two division-independent mechanisms. First, groups of vegetative cells can aggregate on solid surfaces and build spore-filled fruiting bodies (21). Second, individual *M. xanthus* cells can form dispersed, spherical spores in response to chemical signals, such as glycerol (22). Unlike endospores that contain intact and often thickened PG (23, 24), PG is thoroughly degraded during single cell sporulation (25). Without the polarity defined by PG, the mechanism by which glycerol-induced *M. xanthus* spores elongate into rods remains largely unknown.

Results

Two-phase morphological transition during *M. xanthus* spore germination.

Overnight induction by 1 M glycerol produced spores with length to width aspect ratios (L/W) of 1.56 ± 0.36 (n = 789), among which 40.9% are approximately spherical (L/W ≤ 1.3). Overall, the L/W values of most (85.4%) spores were lower than 2. As spores germinated, the morphological transition progressed in a two-phase manner. In the first hour of germination (Phase I), L/W did not change significantly (p = 0.57, Fig. 1A, 1B, *SI Appendix*, Movie S1). After 1 h, L/W increased sharply as the emerging cells transformed into rods (Phase II). 70.2% (n = 198) of emerging cells reached the dimensions of vegetative cells by 3 h (Fig. 1A, 1B, *SI Appendix,* Movie S1, Table S1). After 8 h, the emerging cells are indistinguishable from vegetative cells (L/W = 5.55 ± 1.12, n = 233. Fig. 1A, 1B). Importantly, many oval spores initiated elongation along their short axes (Fig. 1C, *SI Appendix,* Movie S2), indicating that although not perfectly spherical, the geometry of mature spores does not predetermine the polarity of emerging cells.

Using cryo-electron tomography (cryo-ET), we confirmed that mature glycerol-induced spores do not retain PG (*SI Appendix,* Fig. S1). To investigate the role of PG growth in germination, we treated spores with several inhibitors for PG synthesis. In the presence of mecillinam and A22, which inhibit PBP2 and MreB in the Rod system, respectively, spores failed to germinate into rods as their L/W ratios did not increase within 8 h (Fig. 1A, 1B). These treated spores were viable because they were able to grow into rods in inhibitor-free medium. Since A22 and mecillinam-treated spores became even more spherical in Phase I (Fig. 1D), neither inhibitor blocked the

hydrolysis of spore coats that maintain the oval shape of spores. In the presence of cefsulodin that inhibits PBP1A/B, and cefmetazole that inhibits all PBPs except PBP2, spores were able to form rods, albeit the elongation rate was slower (Fig. 1A, 1B). Although not essential for rod-like morphogenesis, aPBPs still contribute to the establishment and maintenance of rod shape. First, L/W values of the cefmetazole-treated spores increased significantly in Phase I of germination ($p < 0.0001$, Fig. 1B, 1D), suggesting that cells elongate earlier when PBP2 is dominant over other PBPs. Second, despite successful elongation in early Phase II (1 – 3 h), 57.2% (n = 215) cefsulodin-treated and 96.6% (n = 203) cefmetazole-treated emerging cells retrogressed to spheres after 8-h treatments (Fig. 1A, 1B). As glycerol-induced spores preserve PG precursors(25), when fosfomycin was added to inhibit the production of UDP-MurNAc, a precursor of PG, spores were able to elongate into rods (Fig. 1A, 1B). Taken together, PG polymerization by the Rod system is essential for the establishment of rod-shape.

We next visualized the patterns of PG growth using a fluorescent D-amino acid, TAMRA 3-amino-D-alanine (TADA) (26) to label newly synthesized PG. To enhance labeling efficiency, we deleted the *dacB* gene (*mxan_3130*), which encodes a D-Ala-D-Ala carboxypeptidase (27). The resulted *ΔdacB* cells showed identical morphology to the wild-type ones and produced sonication-resistant spores. The *ΔdacB* spores showed minor delay in germination and efficient TADA incorporation (Fig. 1E, *SI Appendix,* Fig. S2 and Table S1). Although L/W of spores did not change, PG had started to grow in Phase I. The surfaces of most Phase I spores (78.0%, n = 600) were evenly labeled (Fig. 1E). The remaining 22.0% of spores showed bright patches of

120 TADA on their surfaces (Fig. 1F). However, these TADA patches do not likely register
121 future poles because 47.0% (n = 132) of spores contained more than two such patches
122 and these patches positioned randomly on spore surfaces (Fig. 1G, 1F). In contrast, as
123 cells grew into rods, TADA was incorporated heavily at nonpolar regions and
124 fluorescence signals were generally absent at cell poles (Fig. 1E). The patterns of PG
125 growth indicate that spores first synthesize PG on their spherical surfaces in Phase I
126 and then break symmetry in Phase II by growing PG at nonpolar regions.
127 Neither mecillinam, cefsulodin or cefmetazole was able to block TADA
128 incorporation in Phase I of germination. However, a treatment by all three antibiotics
129 abolished TADA incorporation (Fig. 1H), indicating that both aPBPs and the Rod system
130 contribute to the isotropic PG growth in Phase I. In contrast, mecillinam, but not
131 cefsulodin or cefmetazole, blocked TADA incorporation in Phase II of germination (Fig.
132 1H). Consistent with a recent report that cells reduce their diameter when the Rod
133 system becomes dominant over aPBPs (28), emerging cells continued to grow in length
134 but shrink in width in Phase II (Fig. S3). These results confirm that while both aPBPs
135 and the Rod system participate PG synthesis in Phase I of germination, the Rod system
136 plays major roles in cell elongation in Phase II.
137 **MglA and MglB are required for rapid cell elongation** To investigate how *M. xanthus*
138 spores establish cell polarity *de novo*, we tested the potential roles of polar-localized
139 motility regulators. *ΔmglA* and *ΔmglB* cells were able to form sonication-resistant spores
140 but their spores showed severe delays in elongation during germination. After 3 h, only
141 15.7% of the *ΔmglA* (n= 140) and 10.4% of *ΔmglB* (n = 298) cells reached the
142 vegetative aspect ratio (Fig. 2A, 2B). In contrast, deleting *romR* and *plpA*, the genes

encode another two polar-localized motility regulators (29-31), only caused minor delay in germination (Fig. S4 and Table S1). Both the *ΔmglA* and *ΔmglB* spores were able to elongate in length and shrink in width, albeit at significantly lower rates (Fig. 2A, 2B, *SI Appendix,* Fig. S3), indicating that PG growth by the Rod complex still occurred. Strikingly different from wild-type spores that maintained relatively smooth surfaces during germination, the *ΔmglA* and *ΔmglB* spores generated pronounced bulges at nonpolar regions in Phase II, appearing to have multiple cell poles (Fig. 2A, 2C, *SI Appendix,* Movie S3). However, this crooked morphology was largely corrected after prolonged growth (8 h) (Fig. 2A), implying that a system independent of MglA and MglB was able to generate rod shape, although much less robustly. To determine how MglA and MglB regulate germination, we investigated the spores that expressed the $MglA^{Q82L}$ variant as the sole source of MglA, under the control of the native promoter of the *mglBA* operon. $MglA^{Q82L}$ expresses normally but is unable to hydrolyze GTP (19). Spores expressing wild-type MglB and $MglA^{Q82L}$ showed both a severe delay in cell elongation and bulged surfaces on emerging cells, similar to the *ΔmglA* and *ΔmglB* spores (Fig. 2A, 2B). Thus, the GTPase activity of MglA is required for rapid cell elongation and MglB functions through MglA.

Both the delayed morphological transition and bulged surfaces of the mutant spores suggest that MglA and MglB might regulate PG growth during germination. *ΔmglA ΔdacB* and *ΔmglB ΔdacB* spores were able to grow PG in an isotropic manner in Phase I, identical to the *ΔdacB* spores (Fig. 2D). However, emerging cells from both mutant spores displayed elevated PG growth at cell poles and bulges in Phase II (Fig. 2D). As the Rod complex is the major system for PG growth in Phase II, the MglA-MglB

polarity axis might promote rapid cell elongation by restricting the Rod complexes to nonpolar regions.

MglB determines the first future pole. We expressed endogenous YFP-labeled MglA and mCherry-labeled MglB and correlated their localization patterns with L/W. 94.1% (n = 152) of Phase I spores (L/W $\leq$ 2) contained one or two MglB clusters (Fig. 3A, 3B). In phase II spores (L/W > 2), this ratio increased to 100% (n = 120). In contrast, MglA did not form clusters until Phase II, when 54.2% of emerging cells contained one or two MglA clusters (Fig. 3A, 3B). Thus, during germination, MglB establishes polarized localization before MglA.

To test if the clusters of MglB in Phase I spores mark the polarity inherited from previous vegetative cells, we imaged MglB clusters at 0.05 Hz. the majority of MglB clusters in Phase I spores was highly dynamic (Fig. 3C, *SI Appendix,* Movie S4). Among 114 MglB clusters in Phase I spores, 22.9% remained stationary, and 77.1% showed typical diffusion, with diffusion coefficients (D) of $1.05 \times 10^{-4} \pm 4.62 \times 10^{-5}$ $\mu m^2/s$. These "wandering" MglB clusters were observed in both the approximately spherical (L/W < 1.3) and oval spores (1.3 < L/W $\leq$ 2), which supports our hypothesis that, regardless of their geometry, polarity is not yet established in Phase I spores. As a control, imaged at the same frequency, the fluorescence patches of TADA remained stationary in all spores, which excludes potential artifacts caused by the movements of spores (Fig. 3C, *SI Appendix,* Movie S5).

As germination progressed to Phase II (L/W > 2), the population of diffusive MglB clusters decreased from 77.1% to 23.6% (n = 106, Fig. 3D). Stabilized MglB clusters oscillated between newly established poles (Fig. 3C, *SI Appendix,* Movie S6), which

might provide a mechanism to ensure that MglB occupies each future cell pole for an equal amount of time. When we expressed MglA-YFP in the *ΔmglB* background, the formation of MglA clusters was delayed significantly, and in Phase II of germination, only 23.3% (n = 120) of emerging cells contained MglA clusters (Fig. 3A, 3B). Thus, rods start to form when a wandering MglB cluster stabilizes at one future cell pole and positions MglA to the opposite future pole.

To investigate whether pole-like local cell curvature stabilizes MglB clusters, we quantified the localization of stationary MglB clusters with regard to the geometry of spores. We divide the spore/cell envelope into four quarters. In the quarter that contained stationary MglB clusters, we defined the long and short axes as 0^{o} and 90^{o}, which mark the local curvature that shows the highest and lowest similarity to the poles of vegetative cells, respectively. As shown in Fig. 3E, MglB clusters stabilized randomly in Phase I spores, indicating that MglB stabilizes before the establishment of cell poles and that local curvature does not dictate the stabilized localization of MglB. The population of diffusive MglB clusters decreased dramatically in the presence of A22, mecillinam, cefmetazole and cefsulodin (Fig. 3D), indicating that in Phase I of germination, active PG growth prevents MglB clusters from settling down. After the stabilization of MglB, the sites harboring MglB clusters transformed into poles (0^{o}) in Phase II cells (Fig. 3E).

MglB clusters could stabilize either at the sites where PG synthesis has completed or at the sites where PG synthesis has not yet initiated. We ruled out the second possibility because the majority of MglB clusters (76.4%, n = 106) stabilizes at poles in Phase II (Fig. 3A, 3B), where PG growth has completed (Fig. 1E). Consistent with our

finding that the Rod system becomes the dominant system for PG growth in Phase II (Fig. 1H), A22 and mecillinam further reduced the small population of diffusive MglB clusters in Phase II, while cefmetazole and cefsulodin did not show significant effects (Fig. 3D). Taken together, it is the progress of PG growth, rather than the geometry of the spore, that defines cell polarity. As MglB clusters only stabilize at the sites where PG growth is completed, a region where PG synthesis completes first in Phase I will become a future cell pole.

The MglA-MglB polarity axis regulates PG synthesis by the Rod system through MreB and the gliding motor. MglA and MglB are both cytoplasmic proteins, which are not likely to regulate the enzymatic activities of the Rod system directly. To investigate whether MglA and MglB regulate the distribution of the Rod complexes, we used a fully functional, photoactivatable mCherry (PAmCherry)-labeled MreB variant (17) to mark the localization of Rod complexes in germination Phase II. When the majority of PAmCherry was photoactivated, MreB-PAmCherry appeared as small patches (17) (Fig. 4A). Compared to the wild-type spores where MreB patches mainly localized at nonpolar locations, many MreB patches formed near cell poles and bulges of the emerging *ΔmglA* and *ΔmglB* cells (Fig. 4A). We then photoactivate a few MreB-PAmCherry particles in each emerging cell and quantified their localization using photo-activatable localization microscopy (PALM). Along the long cell axis, we defined a region within 320 nm from each end of cell as the pole and the rest of the cell as the nonpolar region. In the emerging cells from wild-type spores that expressed MreB-PAmCherry, the ratio between nonpolar and polar-localized MreB fractions was 2.68 (n = 573, Fig. 4B). In contrast, in the *ΔmglA* and *ΔmglB* backgrounds, this ratio decreased

to 1.06 (n = 713) and 1.41 (n = 812), respectively (Fig. 4B). Our data support that during the sphere-to-rod transition, MglA and expel MreB, and thus the Rod system, from cell poles.

MglA connects MreB to the gliding motors and the gliding motors drive the movement of MreB filaments (16, 17, 20). To test if MglA recruits the gliding motors to transport the Rod complexes to nonpolar locations through MreB, we investigated the regrowth process of the *ΔaglQS* pseudospores. *ΔaglQS* cells carry truncated gliding motors that are unable to drive the rapid motion of MreB filaments (17). Due to the truncation of motors, the *ΔaglQS* pseudospores lack compact polysaccharide layers on their surfaces (32). Phenocopying the *ΔmglA* and *ΔmglB* spores, elongation of *ΔaglQS* pseudospores delayed significantly and many emerging cells displayed bulged surfaces in Phase II (Fig. 2). Consistently, significantly higher PG growth and MreB localization were observed at cell poles and bulges in the elongation phase (equivalent to Phase II of germination), similar to the observation made in *ΔmglA ΔdacB* and *ΔmglB ΔdacB* spores (Fig. 2D, 4A, 4B). In summary, MglA and mglB restrict PG growth to nonpolar regions in germination Phase II utilizing the gliding motors, which transport the Rod complexes under the control of MglA.

Discussion

As spheres and rods are among the most common shapes adopted by walled bacteria, the sphere-to-rod transition during *M. xanthus* spore germination provides a unique opportunity to study rod-like morphogenesis in bacteria. Due to the absence of PG, glycerol-induced *M. xanthus* spores are especially valuable for the study of *de novo* PG synthesis, which drives spontaneous cell elongation in homogenous environments. In contrast to fruiting bodies that require millions of cells and days to form, glycerol-induced sporulation mimics the natural process that individual *M. xanthus* cells form spores within hours in response to environmental stresses. Without the protection from the fruiting body, rapid elongation could be critical for the survival of individual *M. xanthus* spores.

Based on the mutually exclusive localization of MglB and MglA-GTP in vegetative cells, we propose a model for spontaneous cell elongation during *M. xanthus* spore germination (Fig. 4C). We observed that MglB forms wandering clusters in Phase I of germination. Emerging cells start to elongate when the clusters of MglB stop moving and stabilize at what is to become a future pole. An important clue for understanding this process is that active PG growth prevents MglB clusters from settling down. Thus, the wandering dynamics of MglB clusters serves as a mechanism to survey the status of PG growth and the region where PG growth completes first in Phase I will host a MglB cluster and become a future pole in Phase II. MreB plays a key role in the stabilization of MglB clusters because both MglA and the Rod complexes assemble on MreB. Since MglB avoids colocalizing with MglA-GTP by converting the latter to MglA-GDP (18, 19) and MglA only binds to MreB (which also carries the Rod complexes) in

its GTP-bound form (16), the mutual exclusion between MglB and MglA-GTP will expel MglB clusters from the Rod complexes. Once an MglB cluster stabilizes at one pole, the expulsion between MglB and MglA-GTP causes MglA-GTP to cluster at the opposite side of the spore (Figure 7). Then the diametrically opposing clusters of MglA-GTP and MglB establish the polarity axis of the emerging cell.

A surprising finding of this work reveals that the MglA-MglB polarity axis regulates the distribution of Rod complexes through the gliding machineries. Essential for gliding motility, MreB serves as the platform for the assembly of the gliding machineries (12, 33). For this reason, compared to its homologs in other bacteria, *M. xanthus* MreB displays unique dynamics: it is transported rapidly by the gliding motors, with a maximum velocity of near 3 μm/s (17). At cell poles, MglA-GTP stimulates the assembly of the gliding machinery by directly connecting it to MreB (12, 16). Once assembled, the gliding machineries transport MreB filaments, thus entire Rod complexes, to nonpolar locations (Figure 7) (17, 20). Utilizing the same system that defines the leading-lagging axis in vegetative cells, spherical spores grow their walls at nonpolar regions and eventually form rods.

Consistent with our model, the connection between the Rod complexes and gliding machineries was also observed in a recent report, which showed that PG stops growing in vegetative cells when the gliding machineries are dedicated to gliding (12). The mechanism by which the gliding machineries switch between gliding and PG growth remains to be investigated. Nonetheless, our results have added another layer to the striking versatility of the gliding motors, which transport various cargos in different compartments of the cells: spore coats on cell surfaces (32), the Rod complex and

298 gliding proteins in the membrane and periplasm (12, 15), as well as MreB and gliding

299 proteins in the cytoplasm (12, 17, 34).

Materials and Methods

Strain construction. Deletion and insertion mutants were constructed by electroporating *M. xanthus* cells with 4 μg plasmid DNA. Transformed cells were plated on CYE plates supplemented with 100 μg/ml sodium kanamycin sulfate or 10 μg/ml tetracycline hydrochloride. In-frame deletion of *dacB* is described in *SI Appendix, Materials and Methods, Table S2.*

Sporulation, spore purification and germination. Vegetative *M. xanthus* cells were grown in liquid CYE medium (10 mM MOPS pH 7.6, 1% (w/v) Bacto™ casitone (BD Biosciences), 0.5% yeast extract and 4 mM $MgSO_4$) at 32 °C, in 125-ml flasks with rigorous shaking, or on CYE plates that contains 1.5% agar. When the cell culture reaches OD_{600} 0.1 – 0.2, glycerol was added to 1 M to induce sporulation. After rigorous shaking overnight at 32 °C, remaining vegetative cells were eliminated by sonication and sonication-resistant spores were purified. Sonication-resistant spores were collected by centrifugation (1 min, 15,000 g and 4 °C). The pellet was washed three times with water. More details of spore purification and the purification of *ΔaglQS* pseudospores are provided in *SI Appendix, Materials and Methods.*

Microscopy Analysis. Cryo-ET was performed on a Polara G2™ electron microscope. Images were collected at 9,000× magnification and 8-μm defocus, resulting in 0.42 nm/pixel. Data were acquired automatically with the SerialEM software (35). Time-lapse videos of the germination progress of wild-type and *ΔmglA* spores were recorded using an OMAX™ A3590U CCD camera and a Plan Flour™ 40×/0.75 Ph2 DLL objective on a phase-contrast Nikon Eclipse™ 600 microscope. The length, width and geometric aspect ratios (L/W) of spores/cells were determined from differential interference

323 contrast (DIC) images using a custom algorithm written in MATLAB (The MathWorks,
324 Inc., Natick, MA), which is available upon request. DIC images of spores/cells were
325 captured using a Hamamatsu ImagEM X2™ EM-CCD camera C9100-23B (effective
326 pixel size 160 nm) on an inverted Nikon Eclipse-Ti™ microscope with a 100× 1.49 NA
327 TIRF objective, which are also used for capturing regular fluorescence and PALM
328 images. MglB clusters and single-molecules were localized using an algorithm written in
329 MATLAB (17), which is available upon request. More detailed information is provided in
330 *SI Appendix, Materials and Methods.*

References

1. A. J. Meeske *et al.*, SEDS proteins are a widespread family of bacterial cell wall polymerases. *Nature* **537**, 634-638 (2016).
2. P. D. A. Rohs *et al.*, A central role for PBP2 in the activation of peptidoglycan polymerization by the bacterial cell elongation machinery. *PLoS Genet* **14**, e1007726 (2018).
3. S. van Teeffelen, L. D. Renner, Recent advances in understanding how rod-like bacteria stably maintain their cell shapes. *F1000Res* **7**, 241 (2018).
4. B. P. Bratton, J. W. Shaevitz, Z. Gitai, R. M. Morgenstein, MreB polymers and curvature localization are enhanced by RodZ and predict *E. coli*'s cylindrical uniformity. *Nature communications* **9**, 2797 (2018).
5. A. Colavin, H. Shi, K. C. Huang, RodZ modulates geometric localization of the bacterial actin MreB to regulate cell shape. *Nature communications* **9**, 1280 (2018).
6. S. Hussain *et al.*, MreB filaments align along greatest principal membrane curvature to orient cell wall synthesis. *Elife* **7** (2018).
7. T. S. Ursell *et al.*, Rod-like bacterial shape is maintained by feedback between cell curvature and cytoskeletal localization. *Proc Natl Acad Sci U S A* **111**, E1025-1034 (2014).
8. F. Wong, E. C. Garner, A. Amir, Mechanics and dynamics of translocating MreB filaments on curved membranes. *Elife* **8** (2019).
9. R. M. Morgenstein *et al.*, RodZ links MreB to cell wall synthesis to mediate MreB rotation and robust morphogenesis. *Proc Natl Acad Sci U S A* 10.1073/pnas.1509610112 (2015).
10. H. Cho *et al.*, Bacterial cell wall biogenesis is mediated by SEDS and PBP polymerase families functioning semi-autonomously. *Nat Microbiol* 10.1038/nmicrobiol.2016.172, 16172 (2016).
11. T. K. Lee, K. Meng, H. Shi, K. C. Huang, Single-molecule imaging reveals modulation of cell wall synthesis dynamics in live bacterial cells. *Nature communications* **7**, 13170 (2016).
12. L. M. Faure *et al.*, The mechanism of force transmission at bacterial focal adhesion complexes. *Nature* **539**, 530-535 (2016).
13. E. M. Mauriello *et al.*, Bacterial motility complexes require the actin-like protein, MreB and the Ras homologue, MglA. *Embo J* **29**, 315-326 (2010).
14. B. Nan *et al.*, Flagella stator homologs function as motors for myxobacterial gliding motility by moving in helical trajectories. *Proc Natl Acad Sci U S A* **110**, E1508-1513 (2013).
15. B. Nan *et al.*, Myxobacteria gliding motility requires cytoskeleton rotation powered by proton motive force. *Proc Natl Acad Sci U S A* **108**, 2498-2503 (2011).
16. A. Treuner-Lange *et al.*, The small G-protein MglA connects to the MreB actin cytoskeleton at bacterial focal adhesions. *J Cell Biol* **210**, 243-256 (2015).
17. G. Fu *et al.*, MotAB-like machinery drives the movement of MreB filaments during bacterial gliding motility. *Proc Natl Acad Sci U S A* **115**, 2484-2489 (2018).
18. S. Leonardy *et al.*, Regulation of dynamic polarity switching in bacteria by a Ras-like G-protein and its cognate GAP. *Embo J* **29**, 2276-2289 (2010).

19. Y. Zhang, M. Franco, A. Ducret, T. Mignot, A bacterial Ras-like small GTP-binding protein and its cognate GAP establish a dynamic spatial polarity axis to control directed motility. *PLoS Biol* **8**, e1000430 (2010).
20. B. Nan *et al.*, The polarity of myxobacterial gliding is regulated by direct interactions between the gliding motors and the Ras homolog MglA. *Proc Natl Acad Sci U S A* **112**, E186-193 (2015).
21. D. R. Zusman, A. E. Scott, Z. Yang, J. R. Kirby, Chemosensory pathways, motility and development in *Myxococcus xanthus*. *Nat Rev Microbiol* **5**, 862-872 (2007).
22. M. Dworkin, S. M. Gibson, A System for Studying Microbial Morphogenesis: Rapid Formation of Microcysts in *Myxococcus xanthus*. *Science* **146**, 243-244 (1964).
23. E. I. Tocheva *et al.*, Peptidoglycan transformations during *Bacillus subtilis* sporulation. *Mol Microbiol* **88**, 673-686 (2013).
24. K. Khanna *et al.*, The molecular architecture of engulfment during *Bacillus subtilis* sporulation. *Elife* **8** (2019).
25. N. K. Bui *et al.*, The peptidoglycan sacculus of *Myxococcus xanthus* has unusual structural features and is degraded during glycerol-induced myxospore development. *J Bacteriol* **191**, 494-505 (2009).
26. Y. P. Hsu *et al.*, Full color palette of fluorescent d-amino acids for in situ labeling of bacterial cell walls. *Chem Sci* **8**, 6313-6321 (2017).
27. E. Kuru *et al.*, In Situ probing of newly synthesized peptidoglycan in live bacteria with fluorescent D-amino acids. *Angew Chem Int Ed Engl* **51**, 12519-12523 (2012).
28. M. F. Dion *et al.*, *Bacillus subtilis* cell diameter is determined by the opposing actions of two distinct cell wall synthetic systems. *Nat Microbiol* 10.1038/s41564-019-0439-0 (2019).
29. D. Keilberg, K. Wuichet, F. Drescher, L. Sogaard-Andersen, A response regulator interfaces between the Frz chemosensory system and the MglA/MglB GTPase/GAP module to regulate polarity in *Myxococcus xanthus*. *PLoS Genet* **8**, e1002951 (2012).
30. C. B. Pogue, T. Zhou, B. Nan, PlpA, a PilZ-like protein, regulates directed motility of the bacterium *Myxococcus xanthus*. *Mol Microbiol* **107**, 214-228 (2018).
31. Y. Zhang, M. Guzzo, A. Ducret, Y. Z. Li, T. Mignot, A dynamic response regulator protein modulates G-protein-dependent polarity in the bacterium *Myxococcus xanthus*. *PLoS Genet* **8**, e1002872 (2012).
32. M. Wartel *et al.*, A versatile class of cell surface directional motors gives rise to gliding motility and sporulation in *Myxococcus xanthus*. *PLoS Biol* **11**, e1001728 (2013).
33. B. Nan, Bacterial Gliding Motility: Rolling Out a Consensus Model. *Curr Biol* **27**, R154-R156 (2017).
34. M. Sun, M. Wartel, E. Cascales, J. W. Shaevitz, T. Mignot, Motor-driven intracellular transport powers bacterial gliding motility. *Proc Natl Acad Sci U S A* **108**, 7559-7564 (2011).

421 35. D. N. Mastronarde, Automated electron microscope tomography using robust
422 prediction of specimen movements. *Journal of Structural Biology* **152**, 36-51
423 (2005).
424

ACKNOWLEDGEMENTS

We thank Drs. Joseph Sorg and Ritu Shrestha for their help in the initial determination of germination phenotypes, Drs. Michael Van Nieuwenhze and Yen-Pang Hsu for providing TADA, and Drs. David Zusman, Michael Manson and Joseph Sorg for critical reading of this manuscript. This work is supported by the National Institute of Health R01GM129000 (to B.N.) and R01AI087946 (to J.L.) and by CNRS to T.M.

Figure Legends

Figure 1. PG polymerization by the Rod complex is essential for *de novo* establishment of rod-shape. A) Morphological changes of untreated (UT) and inhibitor-treated wild-type spores in the germination process. Mecillinam (MEC, 100 μg/ml), A22 (100 μg/ml) cefmetazole (CMZ, 5 mg/ml), cefsulodin (CSD, 5 mg/ml) and fosfomycin (FOF, 8 mg/ml). **B)** Quantitative analysis of the germination progress using the aspect ratios (L/W) of spores/cells. Boxes indicate the 25th - 75th percentiles, whiskers the 5th - 95th percentiles. In each box, the midline indicates the median and × indicates the mean (Also see Table S1). Outlier data points are shown as individual dots above and below the whiskers. **C)** Some oval spores initiate elongation along their short axes during Phase II of germination (also see Movie S2). **D)** Phase I spores become more spherical after 1-h treatments by mecillinam and A22 but initiate elongation earlier when treated by cefmetazole. **E)** Patterns of PG growth in both phases of germination were visualized by TADA labeling in *ΔdacB* spores. The average and standard deviation of TADA intensity were calculated from 20 spores/cells in the diagrams to the right (same below). **F)** Imaged at different focal planes, 22.0% of Phase I spores show bright TADA patches (arrows) that position randomly on spore surfaces. **G)** Among these 22.0% spores, many contain multiple TADA patches. **H)** Compared to untreated (UT) *ΔdacB* spores, while neither MEC, CMZ or CSD is able to block PG growth, the combination of all three antibiotics (+3) abolishes PG growth in Phase I of germination. In contrast, MEC alone is sufficient to inhibit PG growth in Phase II. Scale bars, 2 μm. *p* values were calculated using the Student paired *t* test with a two- tailed distribution (same below). NS, nonsignificant difference.

Figure 2. MglA and MglB are required for rapid cell elongation. A) Emerging cells from *ΔmglA*, *ΔmglB, mglA*^{Q82L} spores and *ΔaglQS* pseudospores show significant delay in elongation and crooked morphology in Phase II of germination. **B)** Quantitative analysis of the germination progress. **C)** A representative image of the altered morphology of the emerging *ΔmglA* cells after 3-h of germination. Arrows point to the bulges that appear as additional poles. **D)** The disruption of either the MglA-MglB polar axis (*ΔmglA ΔdacB* and *ΔmglB ΔdacB*) or the gliding motor (*ΔaglQS ΔdacB*) resulted in significantly stronger PG growth at cell poles and budges (arrows) in Phase II. Quantitative analysis of TADA fluorescence is shown on the right. Scale bars, 2 μm.

Figure 3. MglB determines the first future pole. A, B) While MglB-mCherry forms clusters in Phase I spores (L/W ≤ 2), MglA-YFP are largely diffusive in Phase I. Without MglB, MglA-YFP forms significantly less clusters in Phase II. For (**B**), the total number of spores/cells analyzed for each strain is shown on top of the bar. **C)** 77.1% of MglB clusters (red arrow) showed "wandering" dynamics in Phase I spores. In Phase II, MglB clusters (yellow arrow) stabilized at cell poles and oscillated between opposite poles. As a control, a TADA patch (white arrow) on a Phase I spore did not move during the entire imaging process. **D)** The wandering behavior of MglB clusters depends on PG growth as the inhibitors of PG synthesis, A22, MEC, CMZ and CSD, all significantly inhibit the wandering of MglB in Phase I. In contrast, as the Rod system becomes the dominant PG synthesis machinery in Phase II, only A22 and MEC inhibit the wandering of MglB in Phase II. For each treatment, the total number of MglB clusters analyzed is shown on top of the bar. UT, untreated. **E)** The stabilization of MglB clusters at cell poles does not depend on local curvature. Scales bars, 2 μm.

Figure 4. The MglA-MglB polarity axis regulates PG growth through MreB and the gliding motor. A) In the emerging *ΔmglA*, *ΔmglB* and *ΔaglQS* cells in Phase II of germination, MreB patches (arrows) are frequently detected near cell poles and bulges. **B)** The nonpolar-to-polar distribution ratios of MreB molecules were quantified by PALM. For each strain, the total number of MreB particles analyzed is shown on top of the bar. **C)** A schematic model for the *de novo* establishment of rod-shape by the MglA-MglB polarity axis. Scales bars, 2 μm.

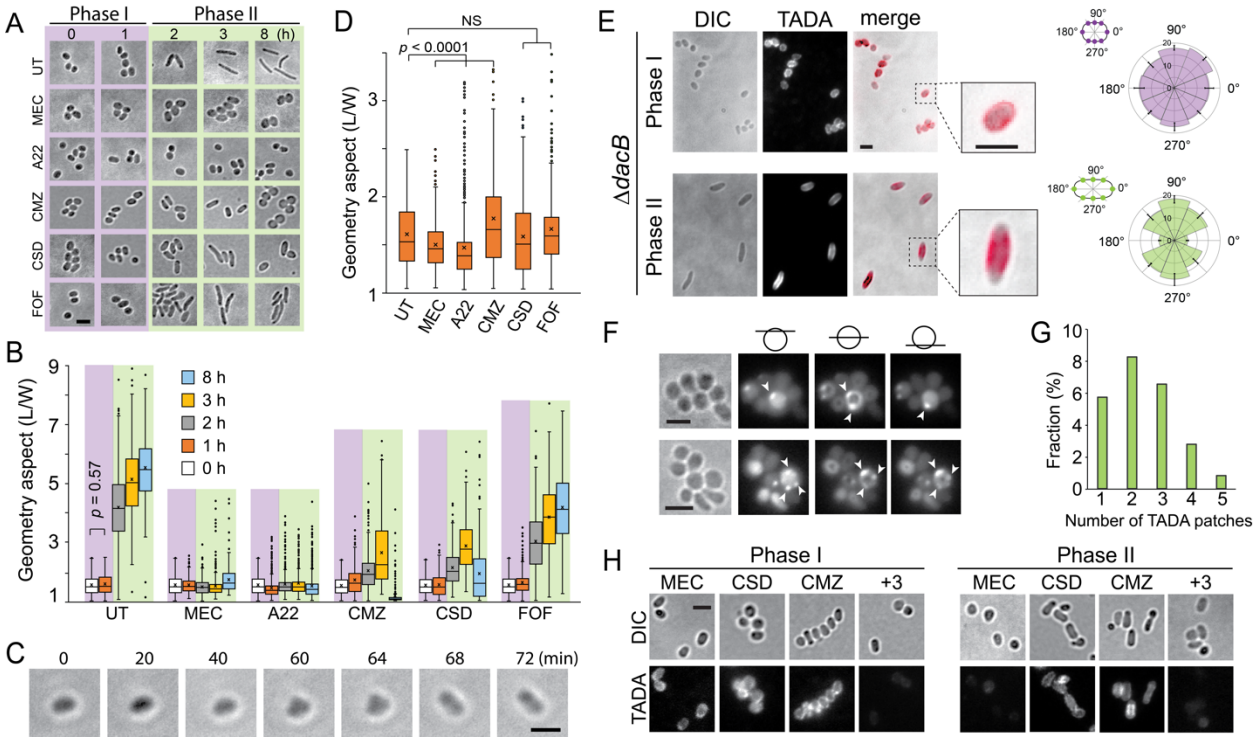

Fig. 1

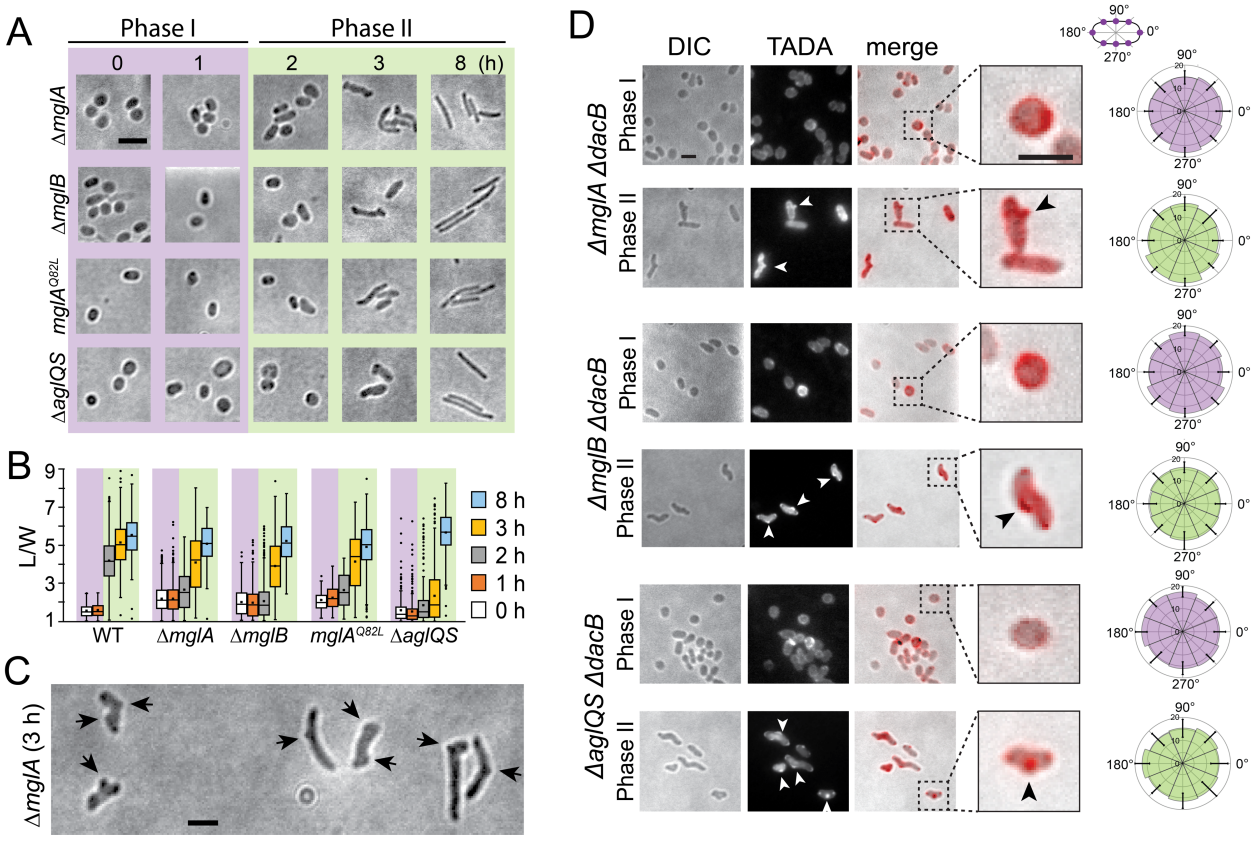

Fig. 2

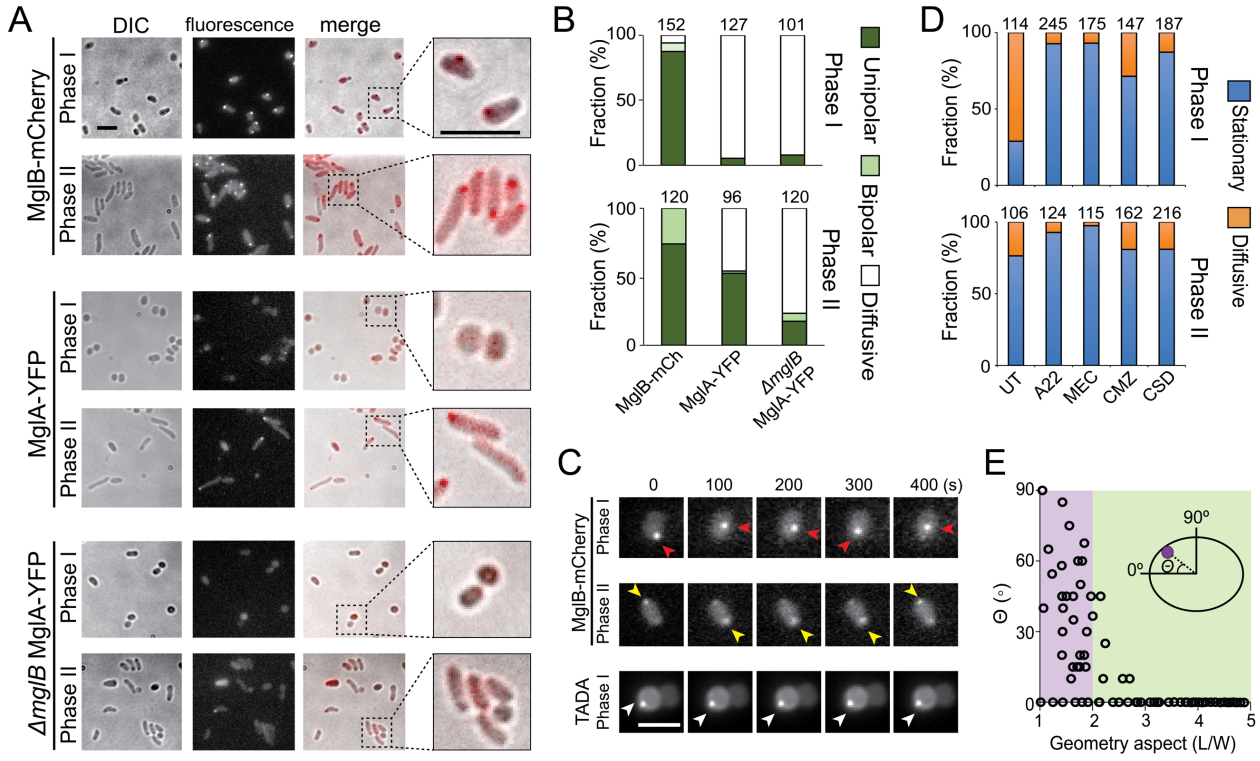

Fig. 3

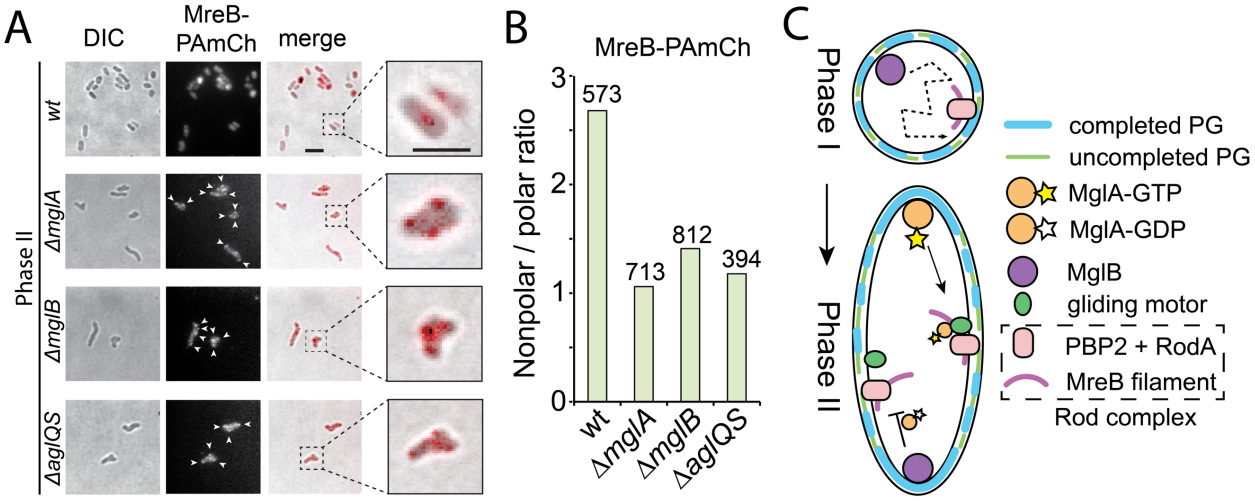

Fig. 4

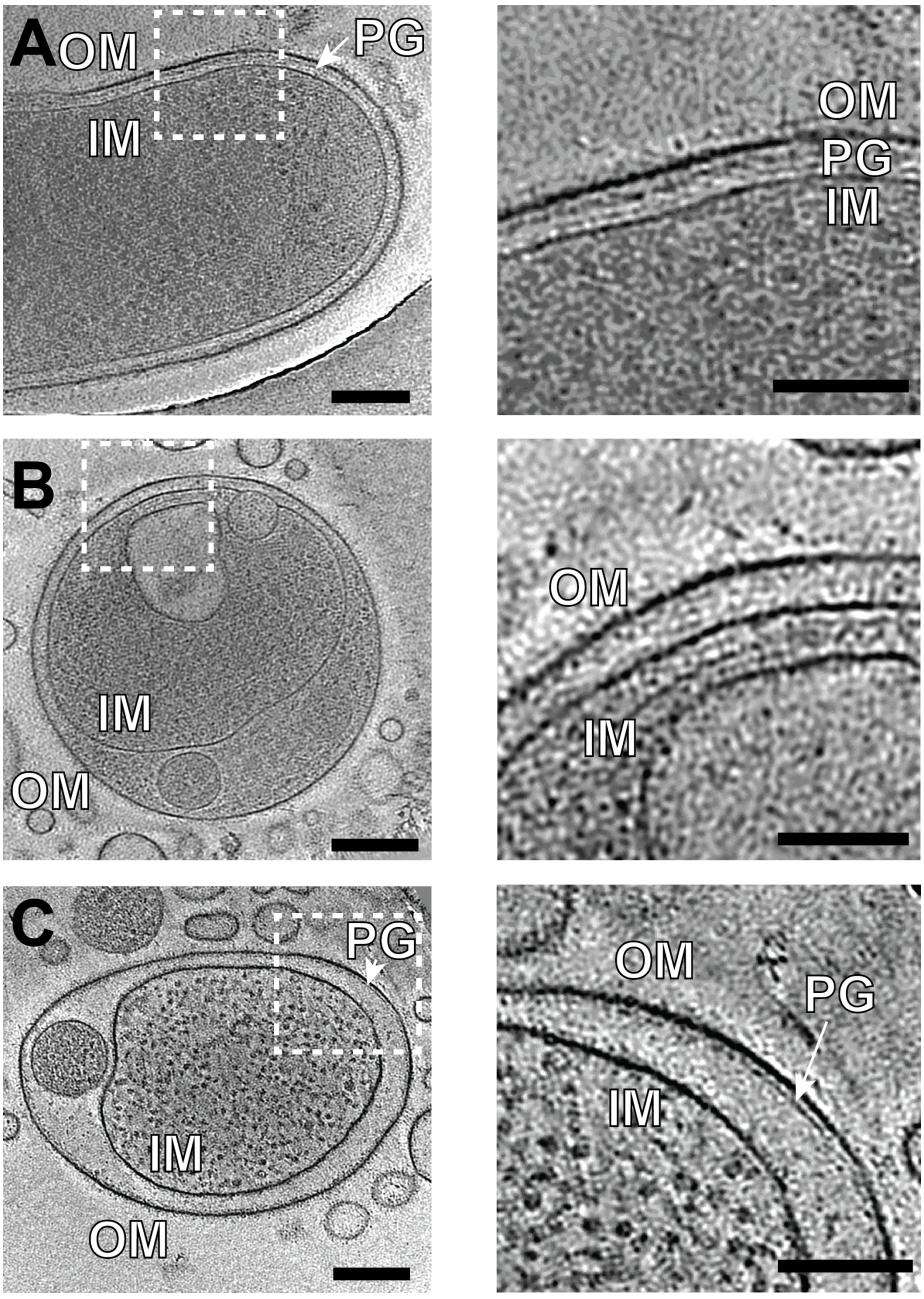

Fig. S1

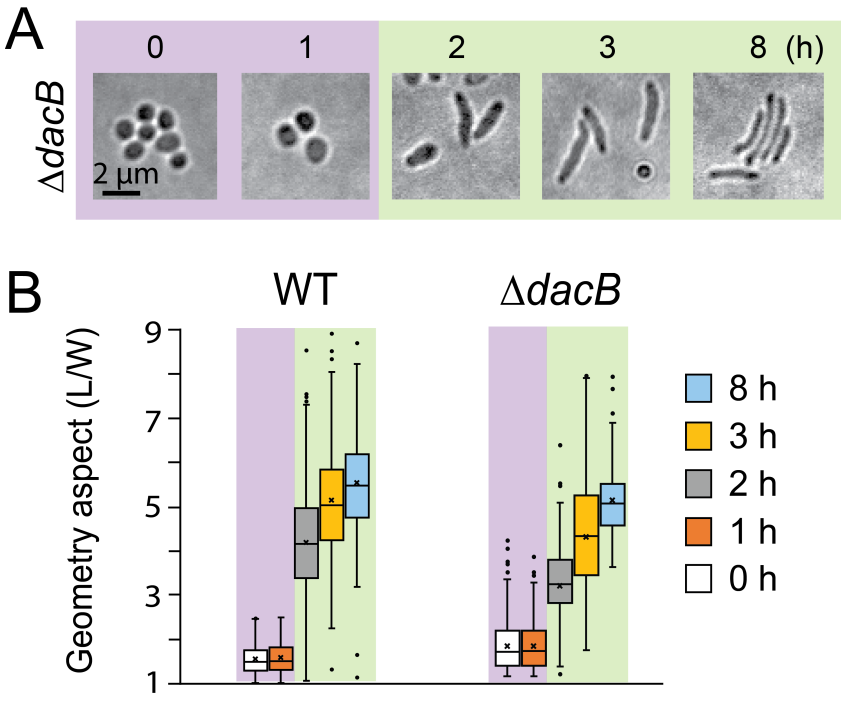

Fig. S2

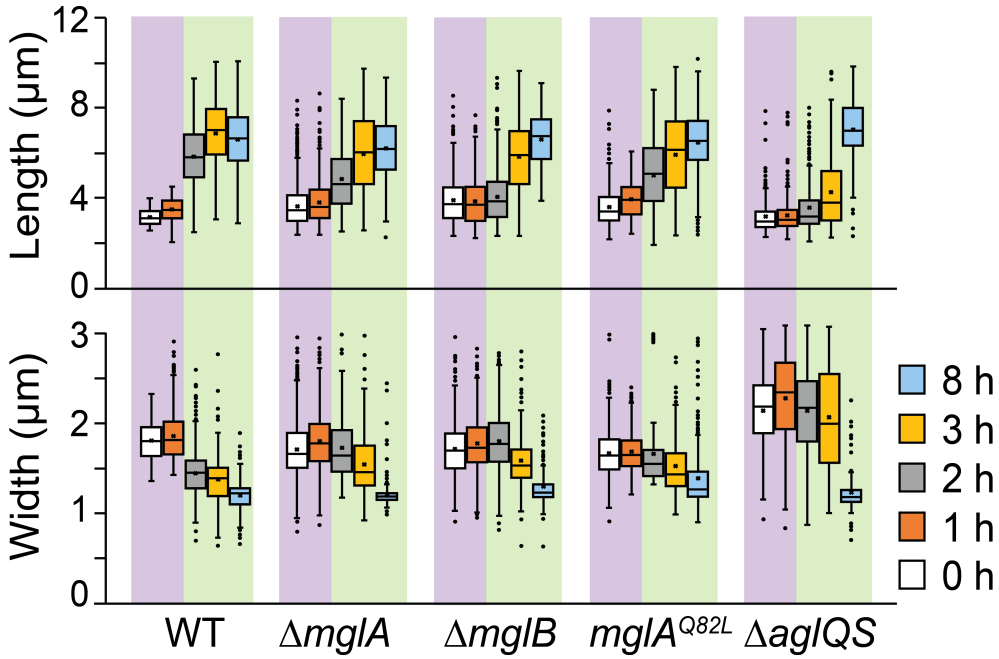

Fig. S3

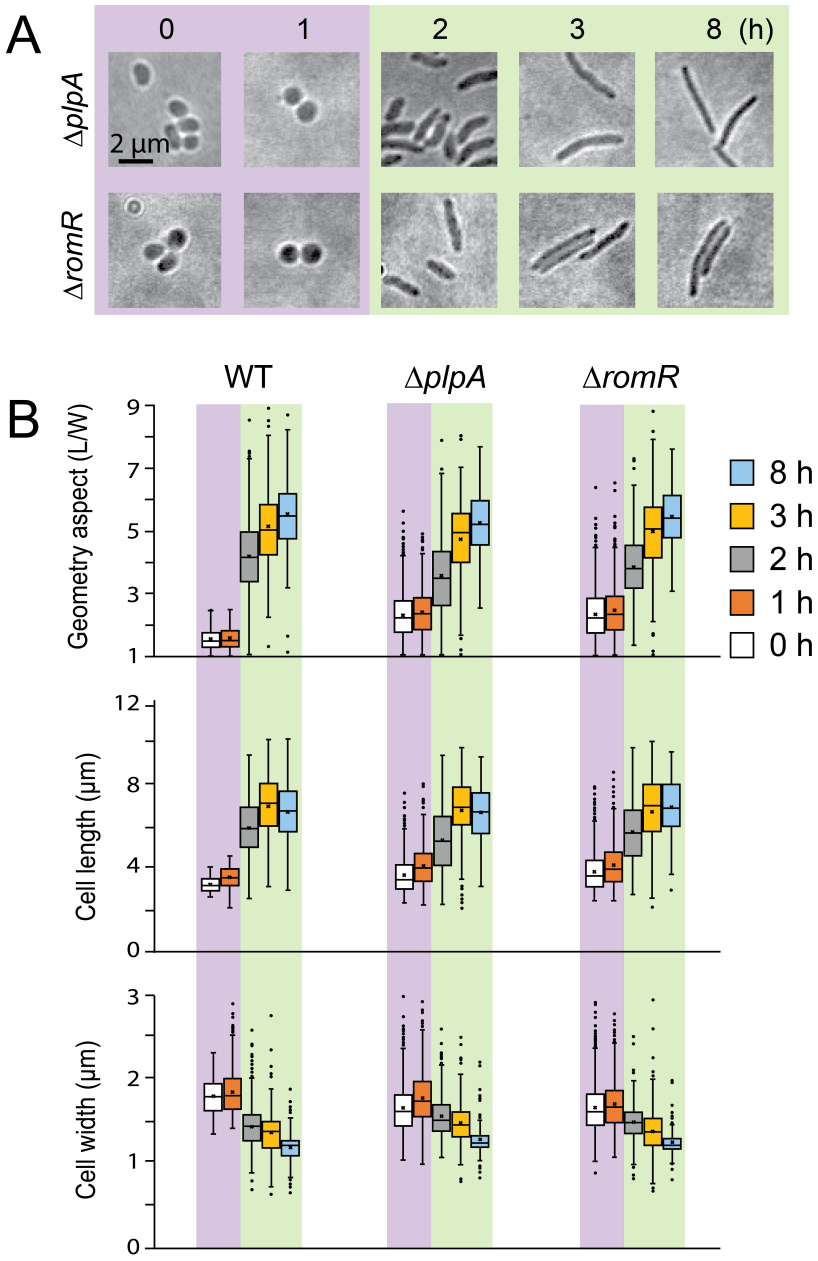

Fig. S4